J. Fluid Mech. (1983), *vol.* 127, *pp.* 353–364
Printed in Great Britain

Boundary-layer transition on a rotating cone in still fluid

By R. KOBAYASHI
Institute of High Speed Mechanics, Tohoku University, Sendai, Japan

AND H. IZUMI
Asahi Glass Co. Ltd, Yokohama, Japan

(Received 25 January 1982 and in revised form 8 September 1982)

A linear stability analysis and experiments were carried out for the laminar–turbulent transition of three-dimensional incompressible boundary layers induced on the surface of a cone rotating around the axis of symmetry with constant angular speed in still fluid. Five cones having total angle of 30°–150° were tested. The results show that the critical and transition Reynolds numbers, the direction of spiral vortices appearing in the transition region and their number on a cone increase as the cone angle is increased, and they tend to the values for the case of a rotating disk. Flow visualizations were made for the transitional process and also for cross-sectional flows of spiral vortices.

1. Introduction

The purpose of this paper is to study the laminar–turbulent transition in three-dimensional boundary layers induced on the surface of a cone rotating in still fluid. A similar transition has already been measured in detail for three-dimensional viscous flow over a circular disk rotating in still fluid by several investigators (Gregory, Stuart & Walker 1955; Chin & Litt 1972; Kobayashi, Kohama & Takamadate 1980; Malik, Wilkinson & Orszag 1981). Although, for rotating cones in still fluid, transition Reynolds numbers were measured by Tien & Campbell (1963) and Kappesser, Greif & Cornet (1973) using mass-transfer techniques, and by Kreith, Ellis & Giesing (1962) using a small microphone and a hot-wire probe, the detailed structure of the transition region has not yet been clarified. In the preceding paper (Kobayashi, Kohama & Kurosawa 1983) attention is mainly devoted to the behaviour of spiral vortices in the transition region on a 30° cone rotating in external axial flow.

The present paper is concerned with the transition on five cones having total angle 30°–150° that are rotating in still fluid. The results are compared with those for a rotating disk as a special case. We present first a linear stability theory and then describe an experiment, carried out for determination of the transition region and for the characteristics of spiral vortices appearing in this region.

2. Theoretical consideration

2.1. *Perturbation equations*

A cone is rotating around the axis of symmetry with a constant angular speed ω in still fluid, as shown in figure 1. It is well known for a rotating circular disk that logarithmic spiral vortices appear in the transition region of flow induced over the disk. By analogy with the rotating disk, we assume that spiral vortices appear as small

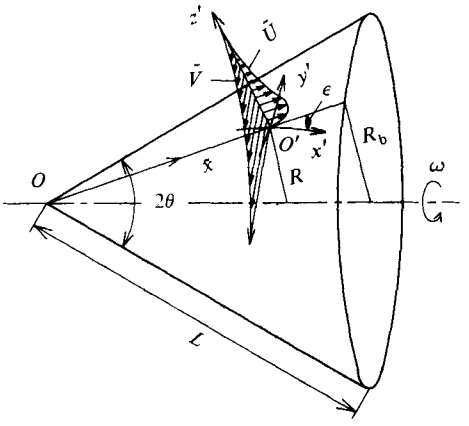

FIGURE 1. Rotating cone in still fluid and coordinate system.

disturbances in laminar boundary layer along the rotating cone having a total angle 2θ, when the boundary layer becomes unstable. We use here an orthogonal curvilinear coordinate system (x', y', z') where the origin O' is fixed on the surface of the rotating cone. The two axes of x' and y' on the surface are set along a pair of logarithmic spirals through the origin O', where they make a right angle. The direction of the y' axis is chosen to coincide with the axis of spiral vortices, so that the x' axis makes an angle ϵ to the meridian of the cone. The z' axis is normal to the cone surface. Because a process for introducing perturbation equations from unsteady Navier–Stokes equations follows closely the one (Kobayashi 1981) for the rotating cone in external axial flow, we give here only an outline of the present linear stability theory. If we denote the x' and y' components of the velocity in the laminar boundary layer by $\bar{U}$ and $\bar{V}$, and the meridional and circumferential components by $\tilde{U}$ and $\tilde{V}$ respectively, as shown in figure 1, then the relations between $(\tilde{U}, \tilde{V})$ and $(\bar{U}, \bar{V})$ are

$$\bar{U} = \tilde{U}\cos\epsilon + \tilde{V}\sin\epsilon, \quad \bar{V} = \tilde{U}\sin\epsilon - \tilde{V}\cos\epsilon. \tag{1}$$

Velocity disturbances of the spiral vortices are given in vector form as

$$\mathbf{v}' = \hat{\mathbf{v}}(z')\, e^{i(\alpha x' - \lambda t)}. \tag{2}$$

The amplitude function $\hat{\mathbf{v}}$ has three components $\hat{u}$, $\hat{v}$, $\hat{w}$ along the x', y' and z' axes. The wavenumber α of the spiral vortices is real; λ is complex, with the real part λ_r related to the phase velocity λ_r/α, and the imaginary part λ_i being the rate of amplification; t is the time. We introduce the following dimensionless expressions:

$$\left.\begin{aligned} z &= \frac{z'}{\delta_1}, \quad U = \frac{\bar{U}}{\omega R}, \quad V = \frac{\bar{V}}{\omega R}, \quad u = \frac{\hat{u}}{\omega R}, \quad v = \frac{\hat{v}}{\omega R}, \quad w = \frac{\hat{w}}{\omega R}, \\ Re &= \frac{\omega R \delta_1}{\nu}, \quad \delta' = \frac{\delta_1}{R}, \quad \sigma = \alpha\delta_1 \sin\theta, \quad c = \frac{\lambda\delta_1}{\sigma\omega R}, \end{aligned}\right\} \tag{3}$$

where δ_1 denotes the displacement thickness calculated by using the circumferential component of the velocity in the laminar boundary layer, R the radius of a local circular cross-section, ωR the local circumferential velocity of the surface, and ν the kinematic viscosity of the fluid. Perturbation equations for the present problem are

then expressed as a system of ordinary differential equations:

$$(U-c)(w_{zz}-\sigma^2 w)-U_{zz}w+\frac{i}{\sigma Re}(w_{zzzz}-2\sigma^2 w_{zz}+\sigma^4 w)$$
$$=\delta'\Big[\frac{i\sin\theta}{\sigma}\{(c-U)\cos\epsilon+V\sin\epsilon\}w_{zz}$$
$$+\Big\{(c-U)\cos\theta-U\cos\theta\sin^2\epsilon+\frac{i}{\sigma}(V_z\sin\epsilon-U_z\cos\epsilon)\sin\theta\Big\}w_z$$
$$-U_z w\cos\theta\cos^2\epsilon+2\cos\epsilon\{i\sigma(V\cos\epsilon-1)\cos\theta-V_z\sin\theta\}v$$
$$+\sin\theta(c\sin\epsilon-2V\cos\epsilon+2)v_z\Big], \tag{4}$$

$$\frac{i}{\sigma Re}(v_{zz}-\sigma^2 v)+(U-c)v-\frac{i}{\sigma}V_z w$$
$$=\delta'\Big\{\frac{i}{\sigma}Uv\sin\theta\cos\epsilon+\frac{\sin\theta}{\sigma^2}(2-V\cos\epsilon+2U\sin\epsilon)w_z$$
$$+\frac{i}{\sigma}\cos\theta\cos\epsilon(V\cos\epsilon-2)w\Big\}, \tag{5}$$

$$i\sigma u+w_z+\delta'\{(u\cos\epsilon+v\sin\epsilon)\sin\theta+w\cos\theta=0, \tag{6}$$

where the subscript z denotes differentiation with respect to z.

The boundary conditions that follow from the requirement of no slip at the wall surface ($z=0$) are $u=v=w=0$. As the other three boundary conditions it is reasonable to take $u, v, w \to 0$ not at an outer edge of the boundary layer but at a point ($z\to\infty$) far from the surface, because the small-wavenumber spiral vortices grow through the outer edge of the boundary layer. In view of the continuity equation (6), the boundary conditions for the perturbation equations (4) and (5) are written as

$$v=w=w_z=0 \quad (z=0), \tag{7a}$$
$$v, w, w_z \to \infty \quad (z\to\infty). \tag{7b}$$

The present linear stability theory is now reduced to an eigenvalue problem for solving the perturbation equations (4) and (5) under the boundary conditions (7), in which the eigenfunctions are $v(z)$ and $w(z)$. After determining the two components $v(z)$ and $w(z)$, the other component $u(z)$ can be obtained from (6). It should be noted that the perturbation equations (4)–(6) are of the same form as those for a rotating cone in axial flow (Kobayashi 1981), when S was put formally equal to unity in the latter (S was the local rotational speed ratio $\omega R/U_e$ and U_e denoted the local flow velocity at the outer edge of the boundary layer). For the numerical procedure for solving the present eigenvalue problem we therefore refer to Kobayashi (1981).

2.2. *Numerical results*

Wu (1959) and Tien (1960) showed under boundary-layer approximations that velocity distributions in the laminar boundary layer along a rotating cone in still fluid can be obtained from Kármán's differential equations for viscous flow on a rotating disk (Kármán 1921). In order to use the velocity field in (4) and (5), we calculated it numerically from Kármán's equations, which gave the displacement thickness $\delta_1 = 1{\cdot}271(\nu/\omega\sin\theta)^{\frac{1}{2}}$. The curvature parameter δ' was then related to the rotational Reynolds number Re by

$$\delta' = \frac{1{\cdot}616/\sin\theta}{Re}. \tag{8}$$

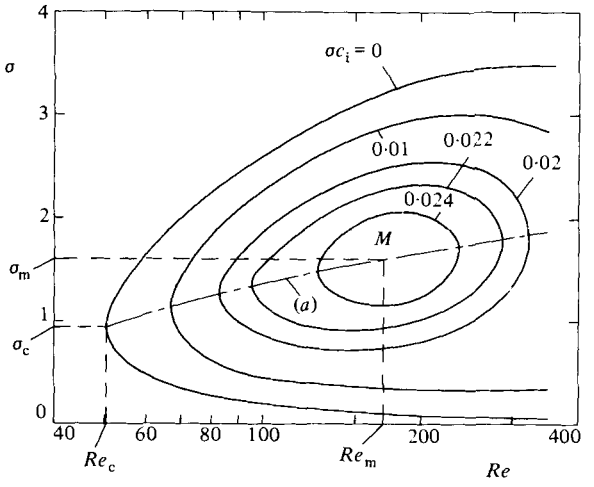

FIGURE 2. Stability diagram for $\theta = 15°$ and $\epsilon = 0°$. Curve (a) shows the σ-values at which the amplification factor σc_i becomes maximum for each value of Re. M is the point at which σc_i becomes maximum for all values of Re. $Re_c = 50{\cdot}5$, $\sigma_c = 0{\cdot}95$, $Re_m = 166$, $\sigma_m = 1{\cdot}6$.

Figure 2 is one of the stability diagrams for a half-cone angle $\theta = 15°$, showing the case $\epsilon = 0°$ for the spiral angle. The parameter $\sigma c_i\,(= \lambda_i \delta_1/\omega R)$ denotes the amplification factor of the vortices, so that the curve for $\sigma c_i = 0$ is in a state of neutral stability and the region for $\sigma c_i > 0$ gives an unstable state. Curve (a) is drawn for the wavenumber σ at which the amplification factor σc_i becomes maximum $(\sigma c_i)_{max}$ for each value of the Reynolds number Re. There exists further the maximum value $(\sigma c_i)_{max}$ along the curve (a) at a certain Reynolds number, namely Re_m, as shown at the point M. The critical Reynolds number Re_c is obtained as the minimum value of Re along the curve of neutral stability ($\sigma c_i = 0$). The two wavenumbers associated with Re_c and Re_m are denoted by σ_c and σ_m respectively.

Figure 3 shows variations of Re_c and Re_m with artificially given values of the spiral angle ϵ. It can be said that both Reynolds numbers Re_c and Re_m vary little as the spiral angle ϵ is changed. Figure 4 shows the maximum amplification factor $(\sigma c_i)_{max}$ for various values of Re and ϵ. The curve (b) represents the values of $(\sigma c_i)_{max}$ for $Re = Re_m$. It should be noted that there exists a maximum of the amplification factor at a certain value of the spiral angle ϵ. In the case of figure 4 for $\theta = 15°$ the angle ϵ is equal to 0°. It might therefore be concluded that the expected angle ϵ of the spiral vortices is $\epsilon = 0°$ in the case of the half-cone angle $\theta = 15°$.

Similar calculations were made for the other cases $\theta = 30°$, 45°, 60° and 75°. The numerical results are given in table 1. In figure 10 the theoretical relation of the spiral angle ϵ to the half angle θ is drawn with a full line. As θ is increased, the spiral angle ϵ increases from 0° up to the value 14·0° for the rotating disk ($\theta = 90°$). In figure 9 a conventional Reynolds number Re_x is used for direct comparisons with experiments. A full line gives the theoretical result, where the Reynolds number $Re_x(= \omega \tilde{x}^2 \sin^2\theta/\nu)$ based on a local radius $\tilde{x}\sin\theta$ of rotation was calculated from the Reynolds number $Re(= \omega R\delta_1/\nu)$ based on the displacement thickness δ_1 by use of the relation $Re_x = 0{\cdot}619Re^2 \sin\theta$. The present analysis shows that the critical Reynolds number $Re_{x,c}$ increases with increasing cone angle θ. Comparisons with experiments will be mentioned in §3.

Figure 5 illustrates streamlines at an unstable state ($Re = 100$, $\sigma = 1{\cdot}4$) for $\theta = 15°$ and $\epsilon = 0°$, which were obtained from the velocity perturbations calculated as

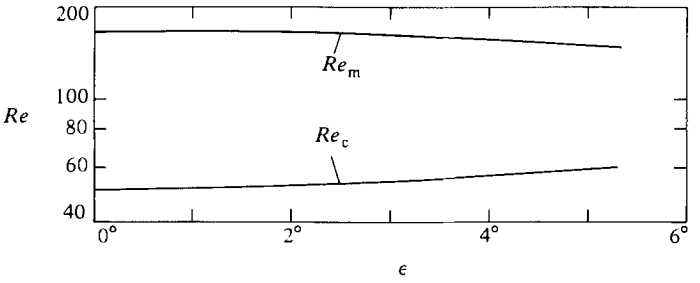

FIGURE 3. Variations of critical Reynolds number Re_c and Reynolds number Re_m for the maximum amplification with artificially given direction ϵ of the spiral vortices; $\theta = 15°$.

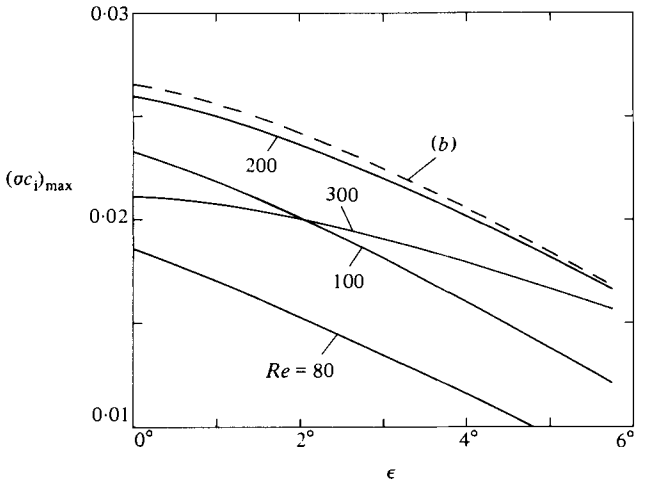

FIGURE 4. Variations of the maximum amplification factor $(\sigma c_i)_{max}$ with artificially given direction ϵ of the spiral vortices; $\theta = 15°$. Curve (b) gives the maximum $(\sigma c_i)_{max}$ at each value of ϵ.

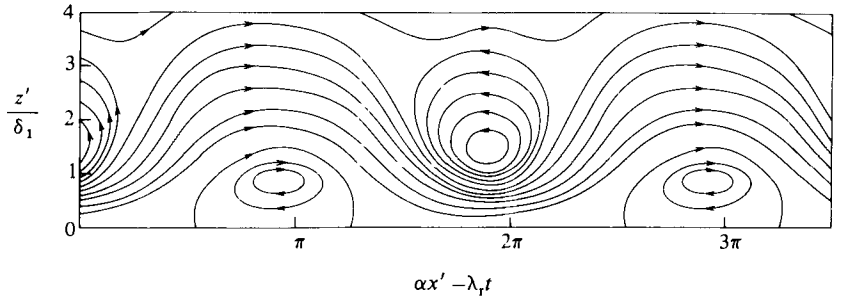

FIGURE 5. Streamlines of the spiral vortices in the boundary layer; $\phi = 15°$, $\epsilon = 0°$, $Re = 100$, $\sigma = 1{\cdot}4$.

eigenfunctions. It is clear that there exists for $\theta = 15°$ one pair of counter-rotating vortices per wavelength. For the case of a rotating disk ($\theta = 90°$), it is known that a unidirectional vortex appears in one wavelength (Gregory *et al.* 1955; Kobayashi *et al.* 1980). It might therefore be said that the type of vortices in the boundary layer of the rotating cone changes from unidirectional vortices to pairs of counter-rotating vortices as the cone angle is decreased from $\theta = 90°$ to 15°.

θ	Re_c Theory	σ_c Theory	Re_m Theory	σ_m Theory	$Re_{x,c}$ Theory	$Re_{x,c}$ Experiment	$Re_{x,t}$ Experiment	ϵ Theory	ϵ Experiment	n Experiment
15°	50·5	0·95	166	1·6	$4·09 \times 10^2$	$1·01 \times 10^3$	$4·87 \times 10^3$	0·0°	0°	
30°	134	0·68	475	0·90	$5·55 \times 10^3$	$9·95 \times 10^3$	$6·15 \times 10^4$	2·7°	1°	
45°	265	0·54	1000	0·64	$3·08 \times 10^4$	$3·74 \times 10^4$	$1·81 \times 10^5$	8·5°	10°	22 ~ 23
60°	310	0·52	1480	0·55	$5·15 \times 10^4$	$6·32 \times 10^4$	$2·68 \times 10^5$	12·5°	12°	26 ~ 27
75°	324	0·50	1700	0·53	$6·28 \times 10^4$	$8·42 \times 10^4$	$3·07 \times 10^5$	13·5°	13·4°	30 ~ 31
90°	332	0·47			$6·82 \times 10^4$	$8·8 \times 10^4$	$3·2 \times 10^5$	14·0°	14°	31 ~ 32

TABLE 1. Numerical data for the transition region of boundary layers induced over the rotating cones in still fluid; data for $\theta = 90°$ are from Kobayashi *et al.* (1980)

FIGURE 6. Flow pattern of boundary layer on a rotating cone in still fluid; $\theta = 15°$.

3. Experiments

3.1. *Apparatus and procedure*

The present experiments were conducted for five test cones having half-angle $\theta = 15°$, 30°, 45°, 60° and 75°. The generation lengths L of the test cones are 173·8 mm for $\theta = 15°$ and 200·0 mm for $\theta = 30°$, 45°, 60° and 75°. The cones were rotated at constant angular speeds around a horizontal axis set at a height of 1065 mm above the floor in still air. The rotating speed can be varied continuously up to 3500 r.p.m. by using a 400 W d.c. motor and a V-belt. The test cones are made of aluminium alloy and finished smooth. We used a hot-wire anemometer to measure the velocity field and also a frequency analyser as the occasion arose. In order to visualize boundary-layer flows, the surfaces of the test cones were painted in black and were spread with titanium tetrachloride.

3.2. *Flow visualizations of the transition region*

We first show photographs visualizing flow patterns over the surface of the rotating test cones in figures 6 and 7. Figure 6 is for half-angle $\theta = 15°$, in which one can see a transition region as stripes, a laminar boundary layer on the left of the transition region and a turbulent boundary layer on its right. Figure 7 is for $\theta = 60°$, in which spiral vortices are clearly observed in the transition region. The test cones in figures 6 and 7 are rotating in the same direction as the cone illustrated in figure 1.

In figure 8, cross-sections of the vortices are made visible by a sheet of strobolight along the meridian of the rotating test cones. In photograph (*a*) for $\theta = 15°$, one observes apparently pairs of counter-rotating vortices as expected in figure 5. The fact that the centre of the right vortex in a pair is nearer to the surface than that of the left vortex agrees qualitatively again with figure 5. Photograph (*b*) for $\theta = 30°$ shows that a vortex appearing at first rotates in the left direction. It is remarked that this direction is the same as the case of a rotating disk (Kobayashi *et al.* 1980). We

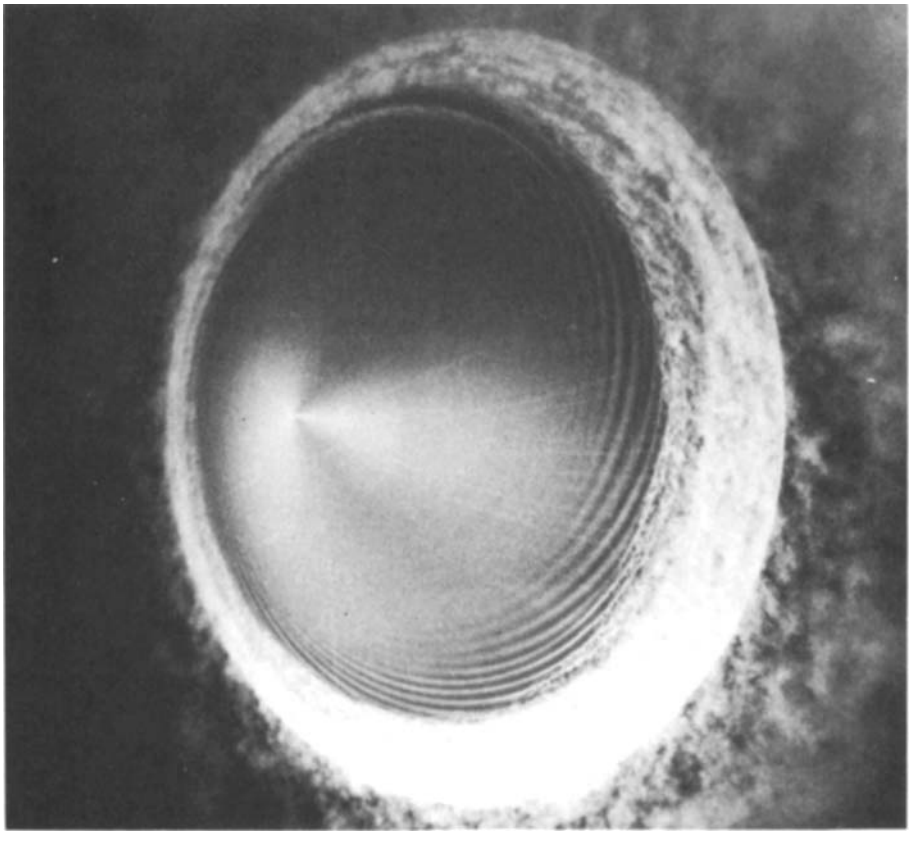

FIGURE 7. Flow pattern of boundary layer on a rotating cone in still fluid; direction of rotation clockwise, $\theta = 60°$.

considered therefore that the pairs of counter-rotating vortices for $\theta = 15°$ might transfer continuously to the unidirectional vortices for $\theta = 90°$ as the cone angle is increased.

3.3. *Critical and transition Reynolds numbers*

As explained in the preceding paper (Kobayashi *et al.* 1983), the critical position $\tilde{x}_c$ of the transition region was measured as the point where periodical signals from the hot-wire probe were detected at a certain frequency in a frequency spectrum. The transition position $\tilde{x}_t$ was defined as the state where velocity fluctuations gave a frequency spectrum for the turbulent boundary layer.

The measured critical and transition Reynolds numbers, defined as $Re_{x,c} = \omega \tilde{x}_c^2 \sin^2\theta/\nu$ and $Re_{x,t} = \omega \tilde{x}_t^2 \sin^2\theta/\nu$, are given in figure 9 and table 1. The values of $Re_{x,c}$ and $Re_{x,t}$ remained constant as the rotational speed N of the cone was varied, which is similar to the case of a rotating disk (Kobayashi *et al.* 1980). In figure 9 the present experiment is compared with previous experiments and also with the aforementioned analysis. Kreith *et al.* (1962) detected the transition region by using a small microphone and a hot-wire probe. Kappesser *et al.* (1973) determined the transition Reynolds number by measuring the mass transfer of oxygen to a rotating cone. Tien & Campbell (1963) also gave $Re_{x,c} = (1{\cdot}3\text{–}1{\cdot}8) \times 10^5$ and $Re_{x,t} = (1{\cdot}4\text{–}2{\cdot}5) \times 10^5$ for $\theta = 45°\text{–}90°$ as well as $Re_{x,t} = 5 \times 10^4$ for $\theta = 30°$ using the

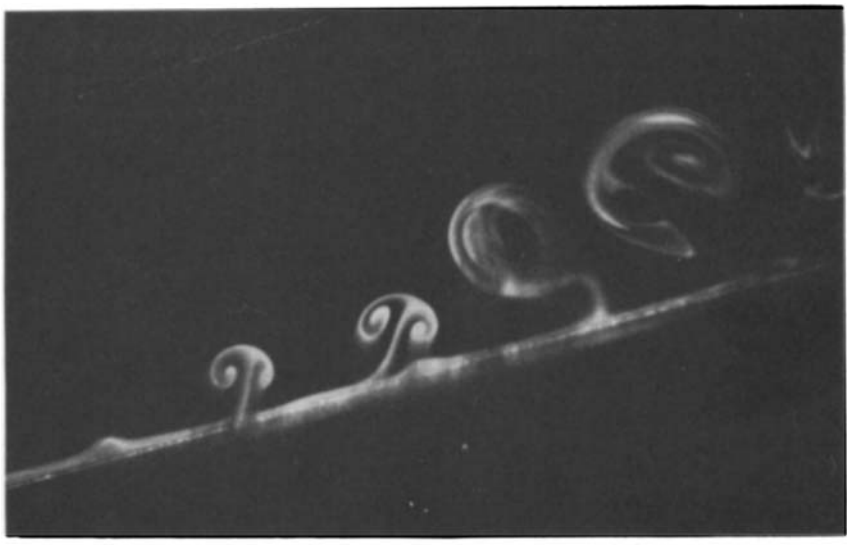

(*a*)

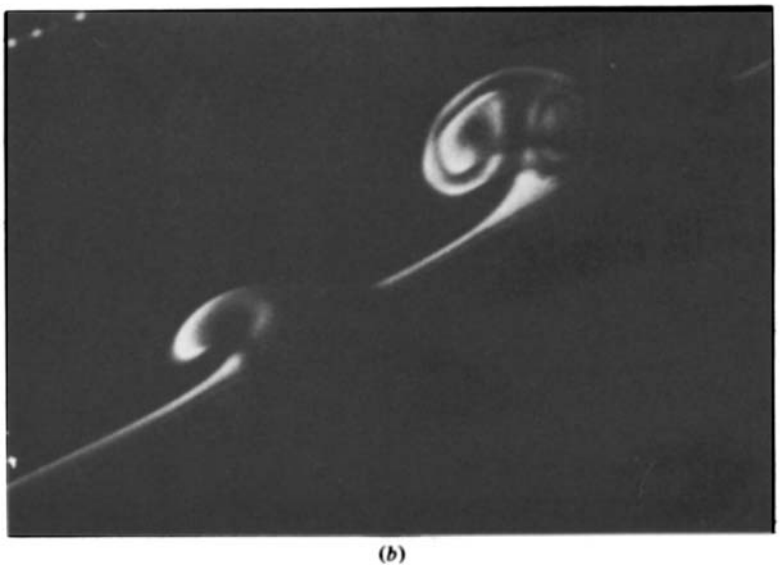

(*b*)

FIGURE 8. Cross-sectional flows of vortices: (*a*) $\theta = 15°$; (*b*) $\theta = 30°$.

mass transfer of naphthalene; these are not shown in figure 9. These previous results are included between the present critical and transition Reynolds numbers shown with two broken lines. The previous values are rather close to the present transition Reynolds number. The differences among the experimenters seem to come from the sensitivity of the detection techniques. It should be noted that the present analysis gives results close to the present experiment. Numerical differences between the present analysis and experiment are given in table 1.

For a rotating cylinder ($\theta = 0°$) in still fluid, Walowit, Tsao & DiPrima (1964) said that the critical Reynolds number $Re_{x,c}$ becomes approximately 11 as estimated from their numerical results of stability analysis for viscous flow between two rotating concentric cylinders. Theodorsen & Regier (1944) gave the transition Reynolds

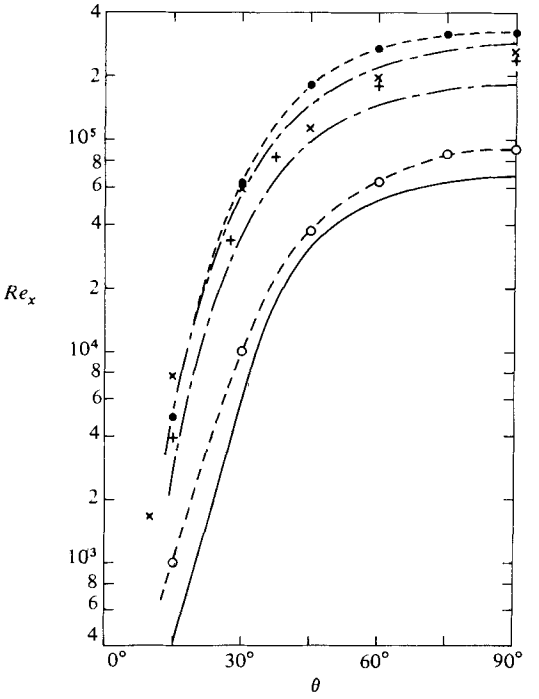

FIGURE 9. Critical Reynolds number $Re_{x,c}$ and transition Reynolds number $Re_{x,t}$. ——, present theory for $Re_{x,c}$. Present experiments: ○, for $Re_{x,c}$; ●, for $Re_{x,t}$. Previous experiments: +, Kreith *et al.* (1962) (small microphone), – – –, Kreith *et al.* (hot wire); ×, Kappesser *et al.* (1973), (mass transfer).

number $Re_{x,t} \approx 10$ by measuring the moment of a rotating cylinder. Flow visualizations by Chen & Christensen (1967) and Kirchner & Chen (1970) showed $Re_{x,c} = 30$. The theoretical and measured results in figure 9 seem to be consistent with these previous values for $\theta = 0°$.

3.4. *Measurements of spiral vortices*

Figure 10 shows the direction ϵ of the vortex axis in relation to the cone angle θ. The angle ϵ was measured directly on photographs of flow visualization, where uncertainty intervals for measurements of ϵ were $\pm 1{\cdot}0°$. The figure indicates that the spiral angle ϵ increases from $\epsilon = 0°$ for $\theta = 15°$ to $\epsilon = 14°$ for $\theta = 90°$ (rotating disk), and that the present theory agrees favourably with the experimental data.

Figure 11 represents the number n of spiral vortices appearing on the test cones, which was measured from many photographs under various conditions of the cone angle and the rotational speed N; for example, in the case of $\theta = 45°$, photographs of 40 sheets were taken, in which 31 sheets gave $n = 22$ or 23 and the other sheets were in a range of $n = 20$–24. The solid line in figure 11 is drawn through the experimental results. It is clear from the figure that the number n of spiral vortices increases as the cone angle θ is increased. For the cone of $\theta = 30°$ it was difficult to measure the number n of vortices, because the direction ϵ of the vortices became about 1°, as shown in figure 10.

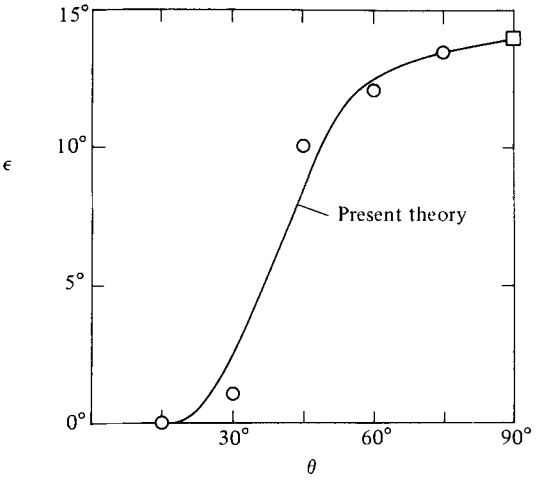

FIGURE 10. Direction ϵ of spiral vortices: □, rotating disk (Kobayashi *et al.* 1980).

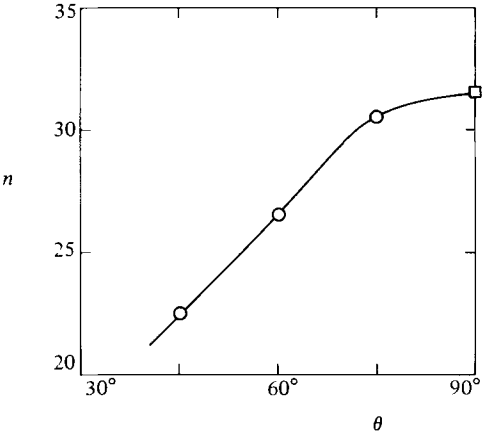

FIGURE 11. Number n of spiral vortices appearing on a rotating cone in relation to the cone angle θ: □, rotating disk (Kobayashi *et al.* 1980).

4. Conclusions

The laminar–turbulent transition region on cones rotating in still fluid was studied by the linear stability theory and the experiment. The results are summarized as follows.

(i) The theoretical prediction that the laminar boundary layer becomes unstable for disturbances of spiral vortex type was confirmed by flow visualizations. The cross-sectional flow of the spiral vortices consisted of pairs of counter-rotating vortices in the case of $\theta = 15°$, while unidirectional vortices appear in the other extreme case of $\theta = 90°$ (rotating disk). We consider that the spiral vortices changes continuously from counter-rotating vortices to unidirectional vortices as the cone angle is increased from $\theta = 15°$.

(ii) The critical and transition Reynolds numbers become larger as the cone angle is increased, as shown in figure 9. The theoretical result for the critical Reynolds

number agrees favourably with the measurement. One of the reasons for differences between both of the critical Reynolds numbers might be the more-complex velocity disturbances at the onset of vortices than the theoretical expression (2), as seen in figure 8.

(iii) The spiral angle increases from $\epsilon = 0°$ for $\theta = 15°$ to $\epsilon = 14°$ for $\theta = 90°$, as shown in figure 10. The number of spiral vortices increases from 22 or 23 for $\theta = 45°$ to 31 or 32 for $\theta = 90°$.

The authors would like to thank Dr Y. Kohama, Institute of High Speed Mechanics, Tohoku University, for his help in the flow visualizations.

REFERENCES

CHEN, C. F. & CHRISTENSEN, D. K. 1967 Stability of flow induced by an impulsively started rotating cylinder. *Phys. Fluids* **10**, 1845–1846.

CHIN, D.-T. & LITT, M. 1972 An electrochemical study of flow instability on a rotating disk. *J. Fluid Mech.* **54**, 613–625.

GREGORY, N., STUART, J. T. & WALKER, W. S. 1955 On the stability of three-dimensional boundary layers with application to the flow due to a rotating disk. *Phil. Trans. R. Soc. Lond.* **A248**, 155–199.

KAPPESSER, R., GREIF, R. & CORNET, I. 1973 Mass transfer to rotating cones. *Appl. Sci. Res.* **28**, 442–452.

KÁRMÁN, T. VON 1921 Über laminare and turbulente Reibung. *Z. angew. Math. Mech.* **1**, 233–252.

KIRCHNER, R. P. & CHEN, C. F. 1970 Stability of time-dependent rotational Couette flow. Part 1. Experimental investigation. *J. Fluid Mech.* **40**, 39–47.

KOBAYASHI, R., KOHAMA, Y. & TAKAMADATE, CH. 1980 Spiral vortices in boundary layer transition regime on a rotating disk. *Acta Mech.* **35**, 71–81.

KOBAYASHI, R. 1981 Linear stability theory of boundary layer along a cone rotating in axial flow. *Bull. Japan Soc. Mech. Engrs* **24**, 934–940.

KOBAYASHI, R., KOHAMA, Y. & KUROSAWA, M. 1983 Boundary-layer transition on a rotating cone in axial flow. *J. Fluid Mech.* **127**, 341–352.

KREITH, F., ELLIS, D. & GIESING, J. 1962 An experimental investigation of the flow engendered by a rotating cone. *Appl. Sci. Res.* **A11**, 430–440.

MALIK, M. R., WILKINSON, S. P. & ORSZAG, S. A. 1981 Instability and transition in rotating disk flow. *A.I.A.A. J.* **19**, 1131–1138.

THEODORSEN, TH. & REGIER, A. 1944 Experiments on drag of revolving disks, cylinders, and streamline rods at high speeds. *NACA Rep.* 793, pp. 367–384.

TIEN, C. L. 1960 Heat transfer by laminar flow from a rotating cone. *Trans. A.S.M.E.* C: *J. Heat Transfer* **82**, 252–253.

TIEN, C. L. & CAMPBELL, D. T. 1963 Heat and mass transfer from rotating cones. *J. Fluid Mech.* **17**, 105–112.

WALOWIT, J., TSAO, S. & DIPRIMA, R. C. 1964 Stability of flow between arbitrarily spaced concentric cylindrical surfaces including the effect of a radial temperature gradient. *Trans. A.S.M.E.* E: *J. Appl. Mech.*, **31**, 585–593.

WU, C. S. 1959 The three dimensional incompressible laminar boundary layer on a spinning cone. *Appl. Sci. Res.* **A8**, 140–146.